Assessment of Unsteady Propagation Characteristics and Corrections in Aeroacoustic Wind Tunnels Using an Acoustic Pulse

Christopher J. Bahr* and Florence V. Hutcheson†
NASA Langley Research Center, Hampton, Virginia, 23681

Daniel J. Stead‡
Science and Technology Corporation, Hampton, Virginia, 23666

Two types of aeroacoustic wind tunnel test section configurations have been tested in the NASA Langley Quiet Flow Facility. The first is a more traditional open-jet configuration, where test section flow passes unbounded through the facility anechoic chamber. The second is the more recent Kevlar wall configuration, where a tensioned Kevlar sheet bounds the test section flow from the facility anechoic chamber. For both configurations, acoustic instrumentation is in the surrounding quiescent space. Both configurations are evaluated with a laser-based pulsed acoustic source, which provides unique capability for assessing the facility unsteady acoustic propagation characteristics. Metrics based on the wander and spread of the pulses are evaluated and show that measurements using Kevlar walls experience dramatically reduced unsteady effects when compared to the open-jet configuration. This leads to a corresponding improvement in coherence between microphones with the Kevlar configuration. Corrections for magnitude and phase for propagation through Kevlar as compared to open-jet propagation are calculated. While limitations in the experimental setup make quantitative analysis difficult, qualitative analysis shows Kevlar magnitude corrections similar to those determined in previous literature. Directivity effects beyond those already present for open-jet configurations are minimal. Phase corrections relative to open-jet configurations are indeterminate within the limitations of the experiment, though data suggest such corrections are not extreme. The background noise produced by the Kevlar is found to be its one drawback when compared with the open-jet configuration, showing significantly greater levels at high frequencies.

I. Nomenclature

CV	=	coefficient of variation
H	=	propagation transfer function
i, j	=	microphone indices
Kev	=	measurement in Kevlar test configuration
$Open$	=	measurement in open-jet test configuration
rm	=	reference microphone
T_{rel}	=	relative transmission coefficient between Kevlar and open-jet configurations
t_a	=	acoustic pulse arrival time
X	=	source signal
Y	=	microphone measurement
Y_0	=	measurement shifted in time by t_a for a given block
$Y_{0,m}$	=	measurement shifted in time by the mean of t_a across all blocks in a record
γ	=	coherence
ϕ_{rel}	=	relative phase angle between Kevlar and open-jet configurations

*Research Engineer, Aeroacoustics Branch, Mail Stop 461, AIAA Senior Member, christopher.j.bahr@nasa.gov
†Senior Research Engineer, Aeroacoustics Branch, Mail Stop 461, AIAA Associate Fellow
‡Senior Engineer, Mail Stop 461

II. Introduction

Aeroacoustic wind tunnels are often configured such that acoustic instrumentation is separated from the facility's test section flow, minimizing measurement contamination by hydrodynamic pressure fluctuations. One facility concept which accomplishes this is the open-jet test section, where instrumentation is separated from the test section flow by a free shear layer [1]. Another facility concept is the Kevlar-walled test section. Here, a sheet of Kevlar constrains the test section flow while allowing acoustic waves to pass through [2]. In both facility types, the acoustic signal of interest must traverse an interface which bounds the test section flow from the quiescent surrounding medium. This boundary influences the propagation of the acoustic waves as they pass through it. In the mean sense, the interface between two media refracts the acoustic waves, leading to a deterministic change in both the direction of wave propagation and the level of the signal [3, 4]. In the unsteady sense, the acoustic signal passes through either a turbulent free shear layer or a turbulent boundary layer on the Kevlar surface. Both classes of turbulent shear flow scatter the acoustic waves of interest, leading to a stochastic change in both the direction of propagation and the level of the signal [5].

The stochastic scattering of the acoustic waves manifests itself in several ways, depending on how the acoustic data of interest are evaluated. In the frequency domain, the scattering can appear as decorrelation, where the level and phase of coherent signals are randomized. This randomization leads to a reduction in average cross-spectral magnitude and, thus, a coherence loss. It can appear as a level reduction for a single microphone when multiple, partially-coherent sources are being measured [6], or as a degradation of the cross-spectra between pairs of microphones for single-source or incoherent field measurements [7–9]. In microphone phased array processing, this degradation can lead to a blurring effect in the source maps, demonstrated in recent airframe noise testing [10, 11]. In the time domain, the scattering can be observed with acoustic pulses as *spread* and *wander*, where spread is defined as a change in pulse form or shape, and wander is defined as a change in pulse propagation time. Wander is considered the dominant mechanism in "weak scattering" assumptions [12, 13], and may be correctable with in-situ techniques [14].

Recently, a cross-facility test campaign utilized a pulsed acoustic source to characterize the influence of flow effects on noise shielding by a canonical airfoil [15–17]. The extensive use of a laser-based plasma source provided an opportunity to study acoustic propagation of pulses through a turbulent shear flow. In the NASA Langley Quiet Flow Facility, microphones were located out of the facility test section to measure the pulsed signal. This was done both for the facility's baseline open-jet configuration, as well as with a Kevlar panel bounding the test section flow on one side. The setup allowed for the direct comparison of the relative influence of both test section interface types on acoustic pulse propagation. This paper proceeds with a discussion of the test setup and data processing, followed by an assessment of the unsteady propagation behavior of pulses through the two interface types. The magnitude and phase corrections for the Kevlar panel are calculated, prior to a brief discussion on the measured pulse spectra. Finally, the background noise characteristics of both test section boundaries are shown.

III. Test Setup and Data Processing

A. Test configuration

The details of the test setup for the overall measurement campaign are provided in the primary NASA-contributed paper for the shielding study [17]. To briefly summarize, an Nd:YAG laser is focused to a point in space, generating a plasma-induced shock wave [18]. This shock propagates and decays to a linear acoustic wave, acting as a nonintrusive acoustic point source. Such a source is particularly appealing for aeroacoustic wind tunnel testing, as most sources placed in a facility test section will alter the test section flow field and generate undesirable aerodynamic noise. In addition to the current noise shielding measurement campaign, this source type has been used in open-jet wind tunnels to evaluate mean refraction effects and mean beamforming corrections [19, 20].

The data used in this study were acquired in the NASA Langley Quiet Flow Facility (QFF). QFF is an anechoic open-jet wind tunnel facility equipped with a 2- by 3-foot rectangular nozzle. For the unsteady propagation portion of this study, the NACA 0012 and inflow microphone from the shielding test were removed. Sketches of the experimental setup are shown in Fig. 1. The Kevlar panel consisted of a sheet of Kevlar 49, Style 120 tensioned to approximately 1500 N/m. Outside of the test section flow, an arc of 1/8" microphones with conventional grid caps was installed. In principle, the setup shown in Fig. 1b would be sufficient to assess the two interface types by comparing instrumentation on opposite sides of the test section. However, comparing the negative angle microphones in Fig. 1a to those in Fig. 1b while maintaining positive angle microphones as references mitigates the influence of minor impulse response differences between individual microphones. This is because, assuming the microphone impulse response functions do not change between configurations, they divide out in the final calculation of relative changes when comparing a given microphone

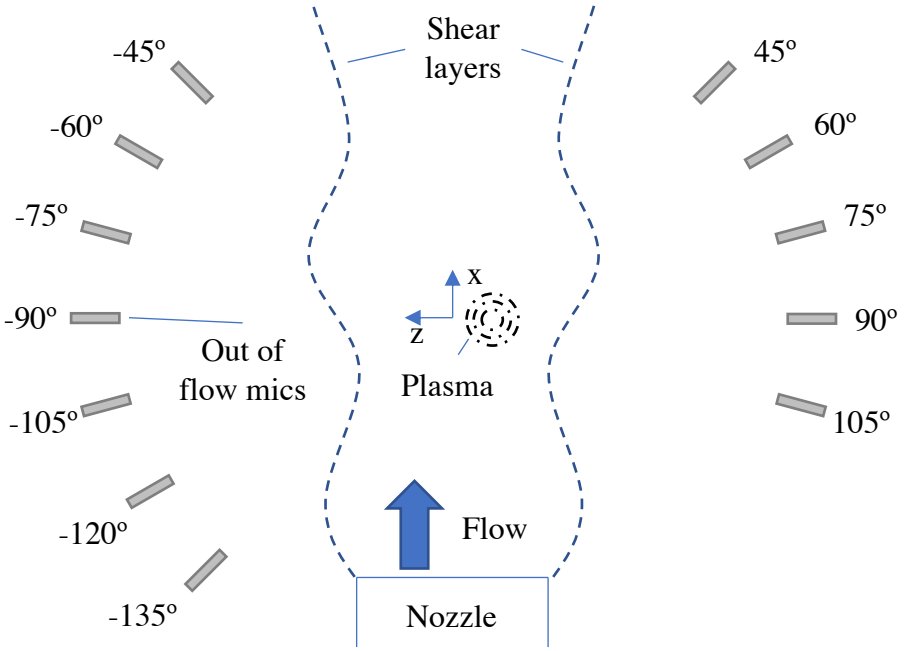

(a) Open-jet configuration

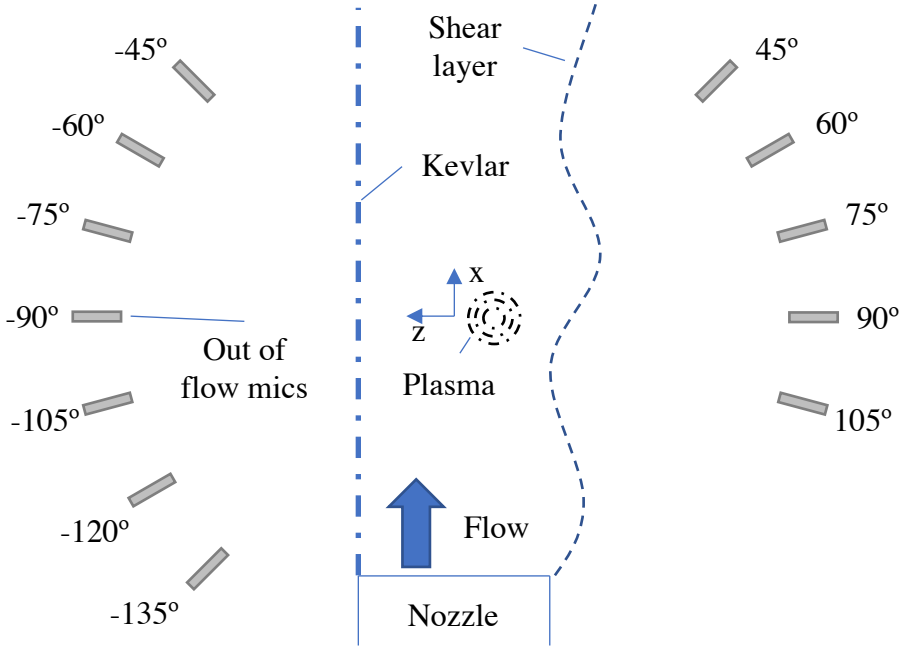

(b) Kevlar panel configuration

Fig. 1 Test section layout for acoustic measurements. Microphone locations are not to scale.

to itself. Also, the lowest microphones could only be installed on one side of the test section.

For a subset of the study, a microphone phased array was also used, though the array measurements with these data are beyond the scope of this paper. Note that the plasma source was not located at the origin of the coordinate system defining the microphone angles, though for the data presented in this paper it was located on the line between the $-90°$ and $90°$ microphones and only 1 inch offset from the origin. This yielded a total error in labeled angle from the true angle of less than $1°$. Also, not all microphones were equidistant from the origin.

B. Data acquisition and processing

All microphone signals were routed through an analog bandpass filter system with a 150 Hz cut-on and 100 kHz cut-off. They were then discretized at a sampling rate of 250 kSamples/s. The q-switch from the laser and a photodetector signal were also routed (unfiltered) to the data system. Data were acquired continuously for 20 seconds, with a laser pulse rate of 5 Hz.

The photodetector was incorporated into the test plan to allow for a more precise measurement of the source pulse initiation, in case there was a delay between the trigger from the q-switch signal and source formation. It also allowed for the detection of misfires, where the laser might pulse but not form a source. This had been observed in some previous work [20]. After the test, it was found that for all inspected data the source formation rate was 100%, and the q-switch and photodetector yielded the same source formation time. The q-switch allowed individual pulse events to be parsed from continuous time records. For these measurement settings, each test configuration acquired either 100 or 101 pulses.

In an effort to improve the pulse-to-pulse alignment of the data referenced to the source formation time, a filtered reference microphone signal and the unfiltered photodetector signal were also routed to a 10 MSamples/s data acquisition card. Having common signals between the 250 kSamples/s and 10 MSamples/s cards allowed for subsample alignment of the lower sampling rate data to the higher sampling rate clock by comparing source formation time measurements between the two systems. This alignment was completed on the higher sampling rate basis by applying a Fourier-based interpolation scheme to the lower sampling rate data. The Fourier-based interpolation method operates by zero-padding the Fourier transform of the lower sampling rate data, and is valid when the signal to be interpolated is filtered such that it is fully represented by its Fourier transform (i.e., no signal components exist above the Nyquist frequency of 125 kHz prior to discretization). The final aligned set of signals was then downsampled to a sampling rate of 1.25 MSamples/s. This sampling rate, being 10 times the Nyquist frequency of the baseline sampling rate, meets the needs of time domain analysis while reducing memory overhead from the 10 MSamples/s data.

The success of this technique is shown in Fig. 2, where measured pulse signals from the reference microphone, here the one located at $90°$ in Fig. 1a, are plotted versus time from source formation for various analysis scenarios. Fig. 2a shows some misalignment of the blocks on the low sampling rate system when superimposing the 100 individual pulses. Fig. 2b shows the benefit of using the higher sampling rate system, as the pulses overlay each other nearly perfectly. Fig. 2c shows the interpolation of the low sampling rate data, which compares favorably to the high sampling rate data. Fig. 2d shows the ensemble average of the individual pulses for each of the three other subplots. The high sampling rate data and the interpolated data ensemble means are extremely close, while the low sampling rate ensemble average has a lower peak level at a slightly different time. Note that the minor change in peak and trough amplitudes between the interpolated and high sampling rate signals is due to the additional anti-aliasing filter present on the low sampling rate data acquisition cards.

It should be noted that for all of these plots, the pulses are not representative of the actual acoustic waveform, which likely has a shape closer to a true N-wave [21]. Rather, they are the pulse waveform distorted by atmospheric attenuation; the diaphragm, grid, and directivity response of the microphone; and the bandpass filter applied to the microphone signal. The microphone grid in particular was observed to add significant distortion to the signal, as has been measured previously [20], and is a strong function of the microphone size and model characteristics. More accurate measurements of the waveform could require alternative measurement methods [22]. Also note that in the final processing of these signals, a 2 kHz phaseless digital highpass filter is applied to the data [23]. This filtering step removes some low frequency fluctuations in the data when test section flow is present.

C. Data analysis

A variety of metrics have been used to characterize acoustic pulses propagating through turbulent media. Arrival time, rise time, peak pressure, and duration have all been considered parameters of interest. However, depending on the degree of waveform distortion these may be non-trivial to determine [24, 25]. The ensemble-averaged acoustic intensity in conjunction with the intensity autocorrelation function are used to model pulse propagation through random media

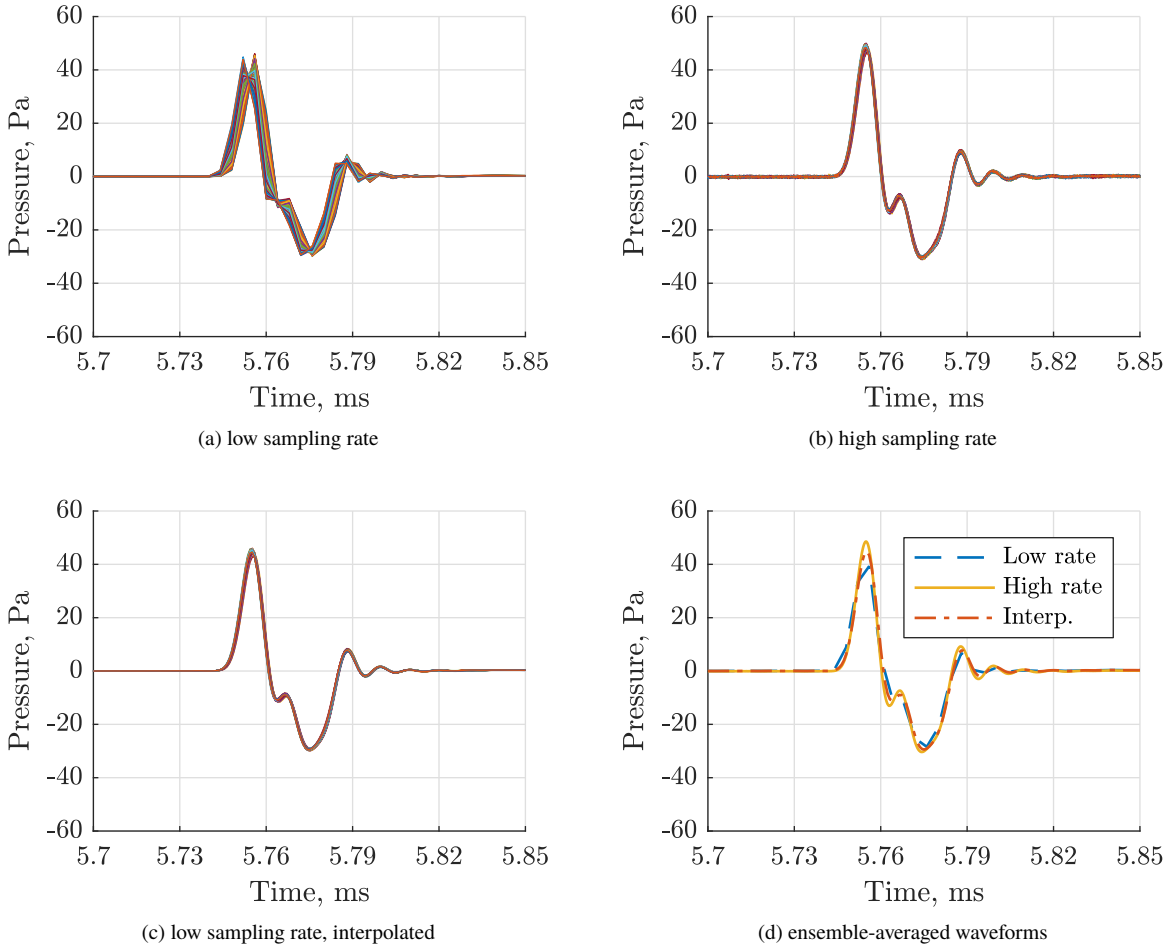

(a) low sampling rate

(b) high sampling rate

(c) low sampling rate, interpolated

(d) ensemble-averaged waveforms

Fig. 2 Comparison of low and high sampling rate block alignment for an example 90° microphone acquisition, without test section flow. Subfigures (a), (b), and (c) show 100 individual pulses aligned to the photodetector signal and superimposed.

and isolate the effects of spread and wander [12, 13].

1. Wander

In this work, wander is directly assessed by extracting the pulse-to-pulse arrival time. The arrival time, t_a, is computed as the first sample in a pulse block to surpass 5% of the peak absolute value of pressure in that block. This definition is found to identify arrival times extremely close to what might be determined from visual inspection of a given block, without falsely identifying a signal fluctuation early in the pulse block.

2. Spread

Spread, or the change in signal shape from pulse-to-pulse, can be assessed by evaluating the frequency-domain behavior of the pulse blocks. Note that prior to any form of Fourier-based analysis, each pulse block is gated with a 600 μs long 25% Tukey window to remove any reflected or scattered signals from the data, reducing analysis to a single propagation path. It is assumed that the gating window, in addition to suppressing these additional signals, also sufficiently attenuates measurement noise such that it can be safely neglected in subsequent analysis. This is because the majority of the block length where the noise would exist is set to zero. The only remaining non-zero data are dominated by the acoustic pulse waveform. For consistency with the associated shielding study, blocks are zero-padded

to interpolate frequency-domain data to a resolution of 61 Hz [17].

Following the general methodology of Pascioni et al. [26], the acoustic signal at microphone i due to an acoustic pulse is given as $Y_i(f) = H_i(f)X(f)$. X, frequency notation subsequently suppressed, is the spectral representation of the source signal while H_i is the complete combination of propagation path, interface, and frequency response effects which influence microphone measurement Y_i. Unlike in the reference, no attempt is made to separate the components of H_i. It is assumed that most contributions to H_i from propagation through the test section potential core and the quiescent air outside of the test section are approximately invariant when compared between the open-jet and Kevlar configurations. Unlike with conventional system analysis, in this work X is assumed to be deterministic while H_i is a random variable with mean and fluctuating components $\overline{H_i}$ and H_i', respectively.

Note that as formulated here, any analysis of H_i will incorporate both the effects of spread and wander, as the randomization of t_a will add further variation to the phase angle of H_i beyond that due to the distortion from spread. As such, the pulse blocks are shifted in time by t_a prior to Fourier analysis. This shift is an attempt to remove the variation due to wander, attempting to isolate the pulse spread in the frequency domain. The resultant formulation, where the arrival time of the pulse is defined as $t_a = 0$ in the shifted time domain, is given by

$$Y_{i,0} = H_{i,0}X = \left(\overline{H_{i,0}} + H_{i,0}'\right)X. \tag{1}$$

With an accurate measurement of X, the behavior of the transfer function could be directly isolated. This is effectively done in the companion work for shielding analysis [17]. In that analysis, direct comparisons using an inflow microphone occur over a small directivity range so the directional response of the instrumentation has a limited effect on the calculated shielding levels. Here, a much wider range of directivity is considered such that the directional response of any inflow microphone measurement cannot be removed when comparing to out of flow microphones. Rather than attempt to correct for the variation of directional response, which can be extreme [27], analysis continues under the assumption that while X is deterministic, it remains unknown.

The sample mean of the shifted transfer function and input can be estimated by ensemble-averaging the shifted, transformed blocks,

$$\overline{Y_{i,0}} = E\left[\left(\overline{H_{i,0}} + H_{i,0}'\right)X\right] = \overline{H_{i,0}}X. \tag{2}$$

The sample variance can then be computed as

$$\overline{|Y_{i,0}'|^2} = E\left[\left(H_{i,0}'X\right)^*\left(H_{i,0}'X\right)\right] = E\left[\left(H_{i,0}'\right)^*\left(H_{i,0}'\right)\right]|X|^2 = \overline{|H_{i,0}'|^2}|X|^2 \tag{3}$$

with * denoting the complex conjugate operation. The influence of the source spectrum can be removed by computing the coefficient of variation. This is done by first computing the magnitude-squared of the mean,

$$|\overline{Y_{i,0}}|^2 = \left(\overline{H_{i,0}}X\right)^*\left(\overline{H_{i,0}}X\right) = |\overline{H_{i,0}}|^2|X|^2, \tag{4}$$

dividing the sample variance by this quantity, and taking the square root,

$$CV_i = \frac{\sqrt{\overline{|Y_{i,0}'|^2}}}{|\overline{Y_{i,0}}|} = \frac{\sqrt{\overline{|H_{i,0}'|^2}}}{|\overline{H_{i,0}}|}. \tag{5}$$

CV, or the coefficient of variation, effectively removes the shape of the source spectrum, along with any instrumentation directivity and atmospheric attenuation effects, from analysis of the transfer function. This is because each microphone measurement is only compared to itself. It should give a frequency-dependent measure of pulse spread. As the ratio of a quantity's standard deviation to its mean, CV gives a measure of the relative influence of variation in a quantity. A CV less than unity would suggest a mean level of a quantity is more significant, while a CV greater than unity would suggest the variation of a quantity is more significant.

3. Coherence

For this test, the coherence-squared between two microphones, $\gamma_{i,j}^2$, is representative of the spatiotemporal decorrelation experienced by the acoustic signal as it passes through a turbulent interface. For an ideal deterministic point source with a single, steady propagation path to each microphone it should be identically unity. For an acoustic

field which has been completely decorrelated, it should be zero. In conventional applications, coherence-based analysis will suffer from the mechanisms that drive both spread and wander. As such, in this work it is computed without shifting the pulses in time. The definition used in this paper then becomes

$$\gamma^2_{i,j} = \frac{E\left[(H_iX)^*\left(H_jX\right)\right]E\left[(H_iX)\left(H_jX\right)^*\right]}{E\left[(H_iX)^*(H_iX)\right]E\left[\left(H_jX\right)^*\left(H_jX\right)\right]} = \frac{|\overline{H_i^*H_j}|^2}{\overline{|H_i|^2}\,\overline{|H_j|^2}}. \tag{6}$$

4. Corrections

Without an accurate measurement of X, it is not possible to directly estimate H_i and therefore not possible to compute a correction for it. However, if a consistent test setup is assumed, a relative magnitude correction between the Kevlar configuration and the open-jet configuration can be calculated. First, the mean-square magnitude for the microphone of interest in the Kevlar configuration is computed,

$$\overline{|Y_i^{Kev}|^2} = \overline{\left(H_i^{Kev}X\right)^*\left(H_i^{Kev}X\right)} = \overline{|H_i^{Kev}|^2}|X|^2. \tag{7}$$

This is then repeated with a reference microphone, herein chosen to be the microphone at 90°. These values are then divided,

$$\frac{\overline{|Y_i^{Kev}|^2}}{\overline{|Y_{rm}^{Kev}|^2}} = \frac{\overline{|H_i^{Kev}|^2}}{\overline{|H_{rm}^{Kev}|^2}}. \tag{8}$$

This process is then repeated for the open-jet configuration, the results divided, and the square root taken to determine a relative transmission coefficient,

$$T_{rel} = \sqrt{\frac{\overline{|Y_i^{Kev}|^2}}{\overline{|Y_{rm}^{Kev}|^2}}\frac{\overline{|Y_{rm}^{Open}|^2}}{\overline{|Y_i^{Open}|^2}}} = \frac{\sqrt{\overline{|H_i^{Kev}|^2}}}{\sqrt{\overline{|H_i^{Open}|^2}}}. \tag{9}$$

A Kevlar panel measurement magnitude is thus divided by T_{rel} to recover the equivalent magnitude of an open-jet measurement for a given microphone location. Using the reference microphone to cancel X accounts for test-to-test variation between facility configuration changes. While these were not observed to be significant, their influence cannot be ruled out. Under the assumption that propagation magnitude effects do not change significantly for the reference microphone from configuration to configuration, the reference terms cancel and leave the Kevlar referenced to the open-jet propagation to microphone i. The instrumentation response, instrumentation directivity, propagation through the test section potential core, and propagation through the quiescent air outside of the test section all cancel under the assumptions of this analysis.

The remaining contributions to T_{rel} are the change in interface from open-jet to Kevlar, the change in shear flow properties along the interface, and atmospheric attenuation. Atmospheric attenuation should be considered due to changes in thermodynamic properties across configuration changes. This can be determined by computing the atmospheric attenuation coefficient [28] and then using Amiet's method to determine inflow and out of flow propagation path distances [4]. The inflow distance is modified with a Galilean transformation to account for convective effects, and then added to the out of flow distance to get an effective emission distance, which is used to compute total attenuation. The total attenuation is then applied as a gain to the microphone spectra Y_i and Y_{rm}. Note that Amiet's method also provides magnitude corrections which could be used to attempt to get an absolute transmission coefficient, but this is not done here.

As with magnitude corrections, phase cannot be directly estimated without an accurate measurement of X. However, unlike with magnitude corrections, relative phase also becomes problematic due to the nature of phase shifts from block to block when flow is present [29]. The analysis presented by Koop et al. requires an accurate measurement of X to estimate a mean phase. When H_{rm} is nearly deterministic such a calculation is still possible,

$$\phi_{rel} = \angle\frac{\overline{Y_{i,0m}^{Kev}Y_{rm,0m}^{Kev,*}}}{\overline{Y_{rm,0m}^{Open}Y_{i,0m}^{Open,*}}} = \angle\frac{\overline{H_{i,0m}^{Kev}}}{\overline{H_{i,0m}^{Open}}}. \tag{10}$$

A Kevlar panel measurement phase thus has ϕ_{rel} subtracted from it to recover the equivalent phase of an open-jet measurement for a given microphone location. Note that the blocks in this calculation are shifted by the mean of the

arrival time t_a prior to analysis. This is because mean propagation times change from configuration to configuration due to changes in the speed of sound from day to day. The remaining contributions to ϕ_{rel} are the change in interface from open-jet to Kevlar and the change in shear flow properties along the interface. When the coherence between microphone i and the reference microphone breaks down per Eq. 6, the phase correction cannot be estimated by this technique.

5. Autospectra and background noise

The autospectra of the acoustic pulses are computed by the traditional method of ensemble averaging the square magnitude of the Fourier transform of each pulse block. This does not provide the noise rejection benefit of ensemble averaging the pulses themselves, but makes the estimate insensitive to wander and less sensitive to spread. These calculations are done without a window function as the blocks have already been gated. The background noise characteristics of the Kevlar panel relative to the open-jet configuration are calculated from data acquired with the laser turned off. These calculations are performed with the standard RMS-average power approach, or Welch's method, using 75% overlap with a Hann window of 4096 points on the 250 kSamples/sec data.

IV. Results and Discussion

Results of the analysis methods of the previous section are now presented. However, prior to delving into these quantitative terms, a brief qualitative discussion of the data is warranted. Individual, source-synchronized pulse waveforms are overlain in Fig. 3 for the $-45°$ microphone with no flow and at Mach 0.17 for both configurations. This microphone is chosen as it should experience the greatest influence of the turbulent shear layers shown in the setup. For clarity, only the first seven waveforms are shown. With no flow, as expected, the waveforms align extremely well. The Kevlar shows a slightly greater t_a than the open-jet configuration, but this is accounted for by the difference in speed of sound from one test to the next, and illustrated with an overlay of Amiet's propagation time prediction. As might be expected, the Kevlar panel does not appear to introduce a significant delay in propagation time when compared to the open-jet. The waveform magnitude is slightly reduced when comparing the Kevlar to the open-jet. With test section flow at Mach 0.17, again the Kevlar shows a slightly greater t_a than the open-jet configuration, which is again accounted for by differences in the speed of sound. The variability of the waveform magnitude and arrival time of the waveform with the Kevlar is much lower than with the open-jet configuration. The open-jet waveforms also appear to suffer significantly more distortion of shape.

As an aside, Fig. 3 may be a helpful illustration of the blurring seen due to decorrelation in microphone phased array processing that was mentioned previously. If data are shifted using Amiet's propagation calculation in time (or the associated phase shift in frequency) for a given grid point in a beam map, the pulses will not align properly from microphone to microphone. Instead, peaks of the waveform from one microphone will line up with off-peak parts of the waveform at a different microphone. Through averaging, this will attenuate the beamformer output at the true source location. However, it can also increase the output at other locations in space. The beam map becomes spatially "smeared."

A. Wander

Wander is herein assessed by comparing the standard deviation of the arrival time, t_a between test section configurations for all the measured angles and Mach numbers. This is plotted in Fig. 4. The wander with no flow is approximately the same between configurations, and is likely a combination of small fluctuations in chamber properties and the temporal resolution of the pulse measurements. When the test section is operated at a finite Mach number, the open-jet configuration wander significantly surpasses that of the Kevlar panel for all Mach numbers and angles. For both configurations, a minimum appears at the upstream angles, progressively increasing in the downstream direction. The Kevlar wander is approximately the same for both Mach 0.13 and 0.17. With rare exception, the open-jet wander continues to increase at all angles with increasing Mach number.

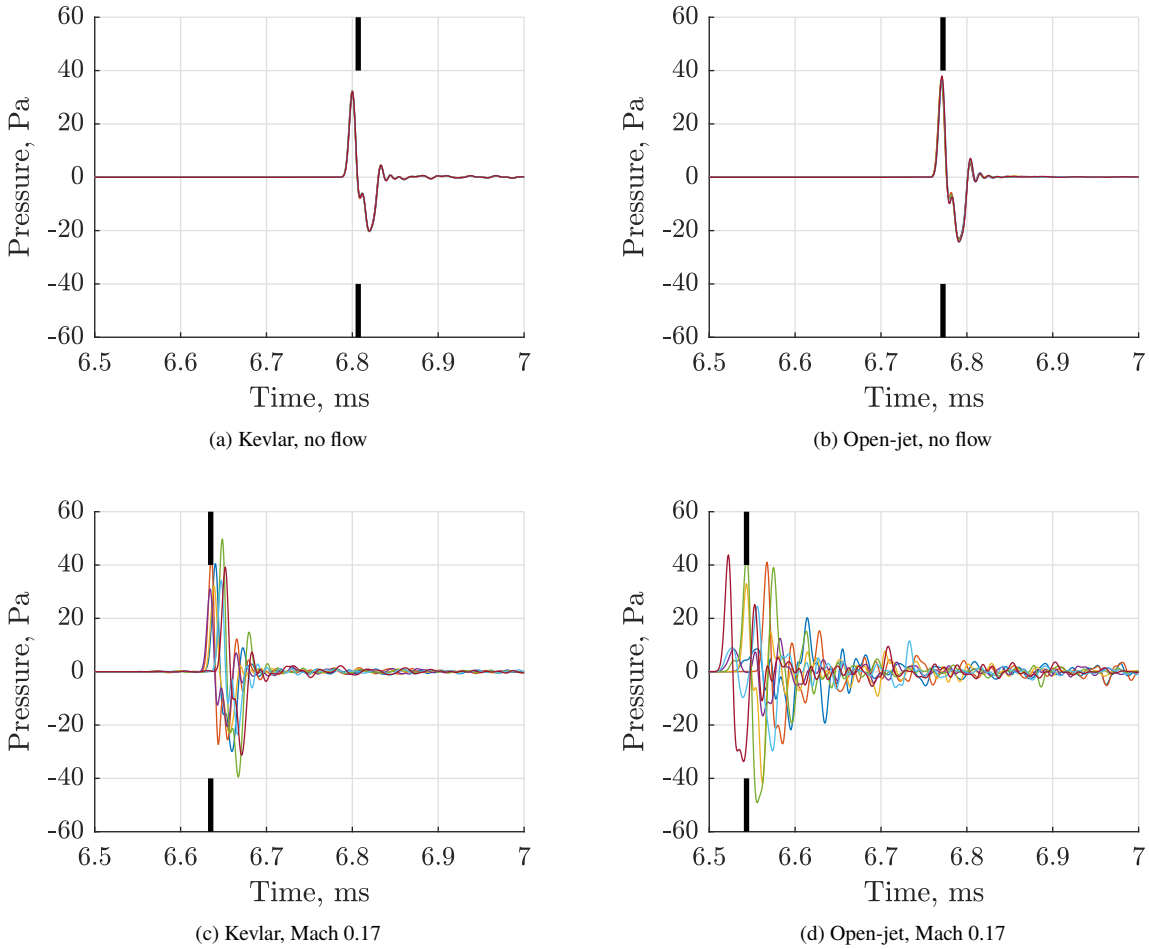

(a) Kevlar, no flow

(b) Open-jet, no flow

(c) Kevlar, Mach 0.17

(d) Open-jet, Mach 0.17

Fig. 3 First seven waveforms acquired in a given test for varying configuration and Mach number, as measured at the −45° microphone. The vertical, broken black line denotes the propagation time prediction from Amiet's method.

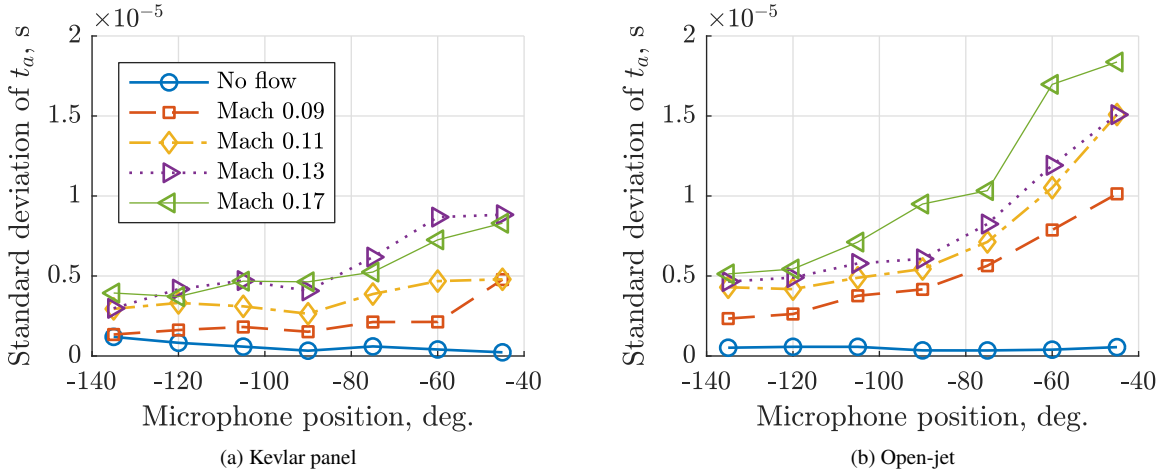

(a) Kevlar panel

(b) Open-jet

Fig. 4 Comparison of standard deviation of arrival time t_a between test section configurations.

B. Spread

Spread, as discussed previously, is assessed by evaluating the coefficient of variation of the spectral data after shifting the individual pulse blocks to mitigate the influence of wander. This spread metric is plotted in Figs. 5 and 6. Frequency plot bounds are selected with the digital highpass filter as the lower bound and the analog lowpass filter as the upper bound. As with wander, the spread of the pulses with no flow is approximately the same between configurations. When the test section is operated at a finite Mach number, the open-jet configuration spread significantly surpasses that of the Kevlar panel for all Mach numbers and angles. Spread increases as a function of frequency in all the data. Individual peaks appear in some spread calculations, but no attempt is made to assign physical meaning to these peaks beyond general data trends.

At its worst, the Kevlar panel spread approaches a CV of 0.5 at the $-45°$ microphone for a Mach number of 0.17. These low CV values suggest that most propagation through the Kevlar panel is dominated by mean effects once wander has been removed, rather than by fluctuating effects. Conversely, the spread of the open-jet data always reaches unity at high frequencies for a Mach number of 0.17. Additionally, at the downstream angles of $-60°$ and $-45°$, CV reaches values of 10 or greater at high frequencies, and surpasses unity below 20 kHz. This suggests that, at these downstream angles, a signal with high frequency content is dominated by fluctuating effects once wander has been removed, rather than by mean effects. Thus, for the Kevlar panel, weak scattering may be a safe assumption. For the open-jet configuration, downstream propagation at higher test section Mach numbers appears to experience strong scattering.

C. Coherence

The coherence between channels is now considered. The microphone at $-90°$ is used as the reference microphone for coherence calculations, and all other microphones on the same side of the Kevlar panel or free shear layer are analyzed. The coherence plots are shown in Figs. 7 and 8, separated by downstream and upstream angles. Coherence is not quite unity as it would be under ideal no flow conditions. At high frequencies there is a minor roll-off. This may be due to small fluctuations in thermodynamic properties, or possibly to minor free convection in the facility.

As with the other unsteady metrics, for all finite flow speeds the Kevlar panel shows improved behavior when compared to the open-jet configuration. Interestingly, the Kevlar shows improved coherence behavior when comparing the Mach 0.13 data to the Mach 0.17 data. This would appear to be in agreement with the wander data shown in Fig. 4a, where for many angles the wander is nearly the same when comparing those Mach numbers. If coherence roughly trends with wander for the Kevlar panel, this might further support a weak scattering assumption for this test configuration. The open-jet data show far more coherence reduction for a given angle and Mach number, dropping as low as $\gamma^2 = 0.2$ at 10 kHz for the $-45°$ microphone at Mach 0.17.

D. Corrections

The computed correction factors are shown in Figs. 9 and 10. The magnitude correction factors show significant fluctuation. This has been reported previously with other wind tunnel installations [2], though much cleaner results with a pulsed laser source have also been obtained [26]. Some of this fluctuation may be attributed to the response of the Kevlar itself. Comparing Fig. 3a to Fig. 3b, it is evident that some ringing is present in the signal after the initial pulse arrival for the Kevlar configuration and that this ringing does not appear to change from block to block. This is not the case for the open-jet configuration, and may be due to the structural response of the Kevlar installation. Another factor, Doppler shift, also appears to affect the downstream angles. This will be discussed with the signal autospectra.

Considering overall trends and neglecting peaks in the plots, the magnitude correction is slightly lower than in other references for their reported frequency ranges. While other work has reported a velocity dependence in the magnitude correction factor for Kevlar, it is not observed here. This is likely because in this work the Kevlar is referenced to a free shear layer, which already has a velocity-dependent correction factor [4]. The overall relative magnitude correction factor for the Kevlar does not show a strong angle dependence in trends, indicating that whatever directionality is present trends the same as the free shear layer directionality.

As mentioned previously, phase corrections suffer dramatically when coherence is low due to spread and wander of the acoustic pulses. In these plots, the relative phase correction is shown only where γ^2 between microphones i and rm for both the Kevlar panel and open-jet configurations is greater than 3%. For the 100 blocks of data acquired, this corresponds to a standard deviation in mean phase angle estimate of 23° [30]. Additionally, dashed black lines are superimposed over the data to illustrate the effect on phase correction if the t_a shift was off by 1 sample, as computed for 1.25 MSamples/s. With all of this, it is very difficult to draw any conclusions regarding the phase correction of

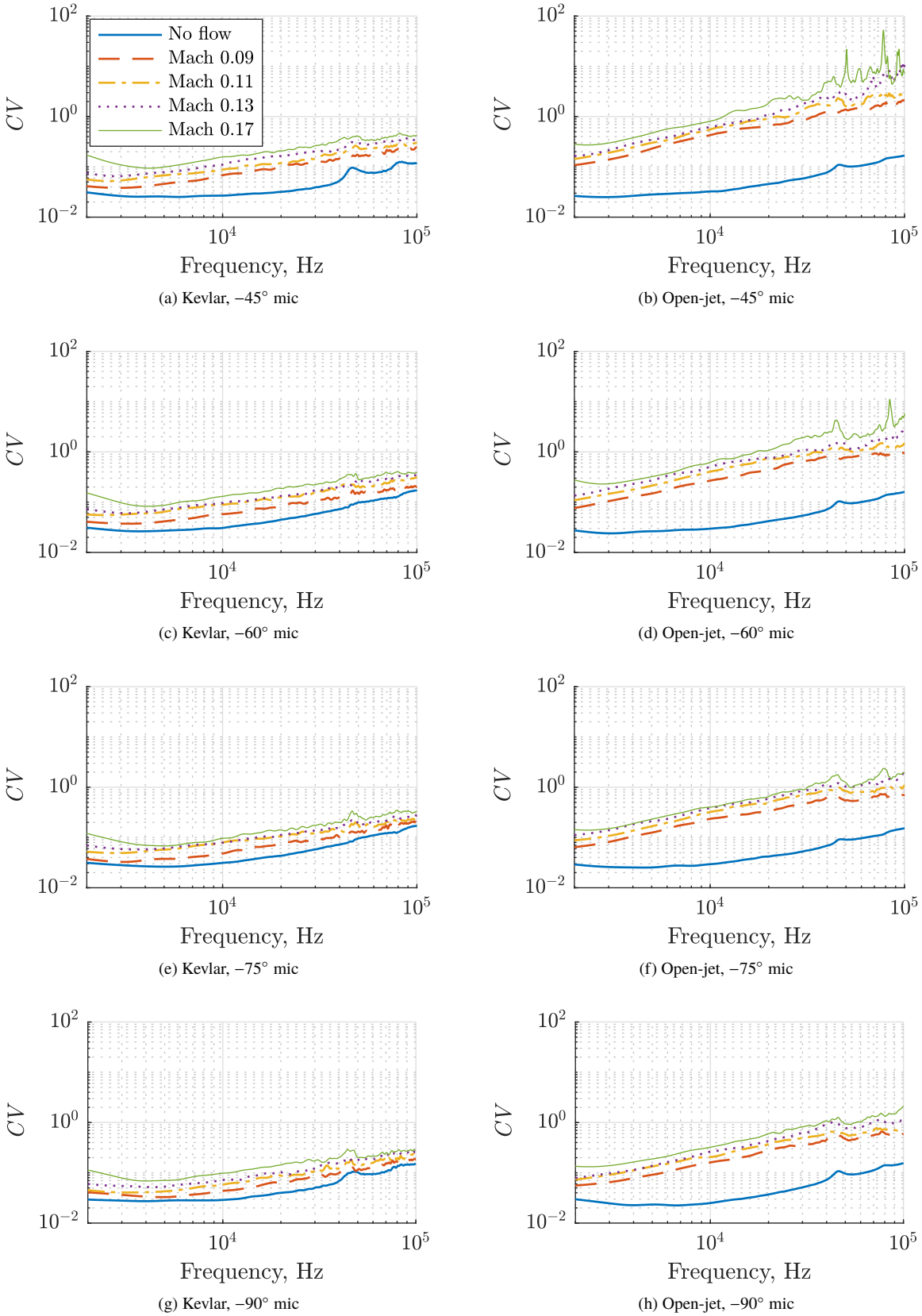

(a) Kevlar, −45° mic

(b) Open-jet, −45° mic

(c) Kevlar, −60° mic

(d) Open-jet, −60° mic

(e) Kevlar, −75° mic

(f) Open-jet, −75° mic

(g) Kevlar, −90° mic

(h) Open-jet, −90° mic

Fig. 5 Comparison of CV as a function of frequency between test section configurations for downstream angles.

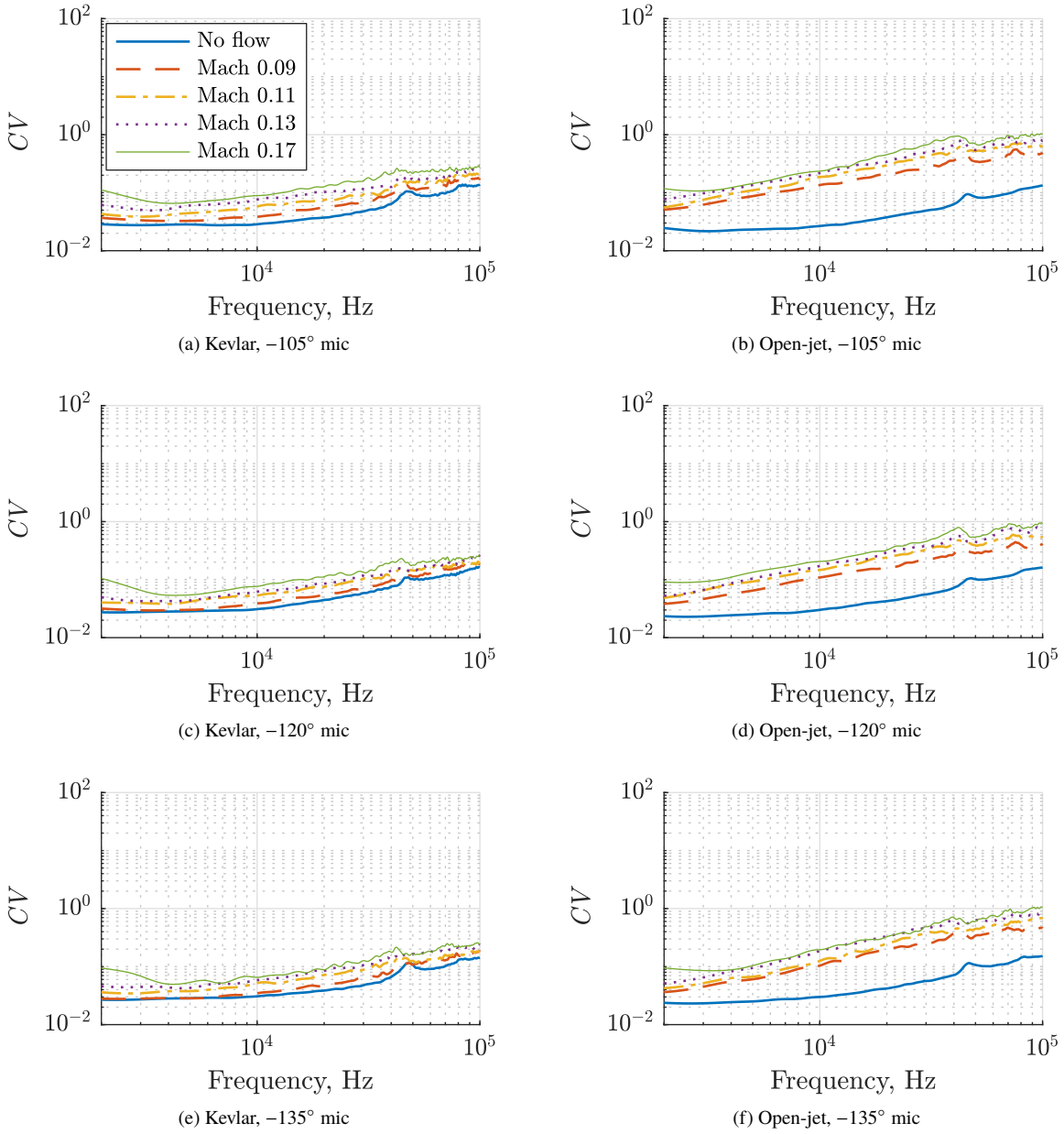

(a) Kevlar, −105° mic

(b) Open-jet, −105° mic

(c) Kevlar, −120° mic

(d) Open-jet, −120° mic

(e) Kevlar, −135° mic

(f) Open-jet, −135° mic

Fig. 6 Comparison of CV as a function of frequency between test section configurations for upstream angles.

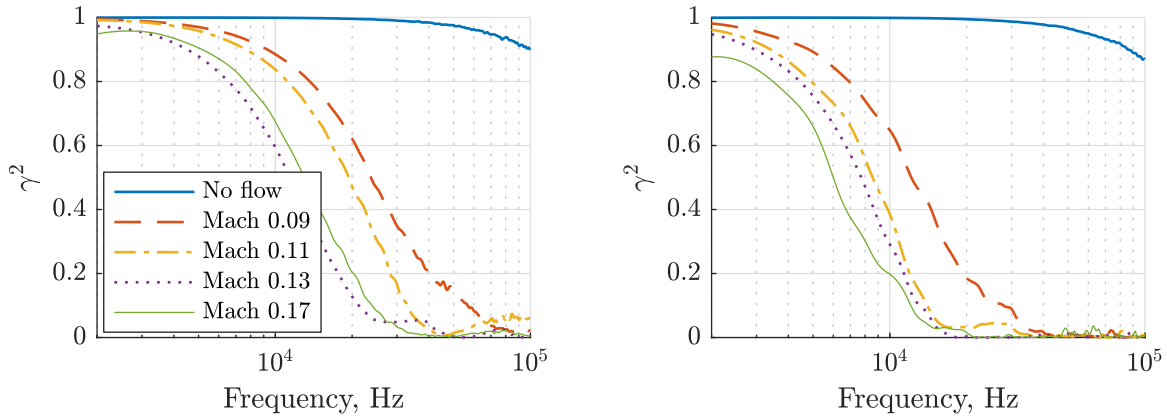

(a) Kevlar, −45° mic

(b) Open-jet, −45° mic

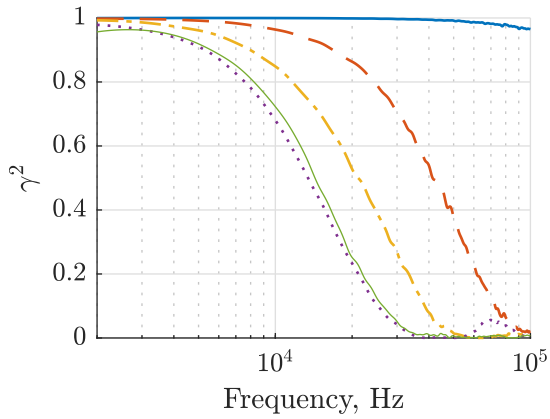

(c) Kevlar, −60° mic

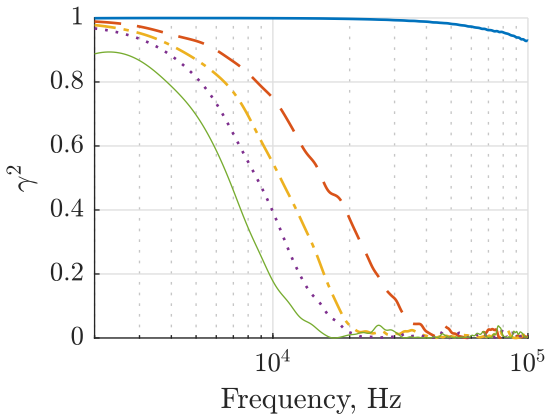

(d) Open-jet, −60° mic

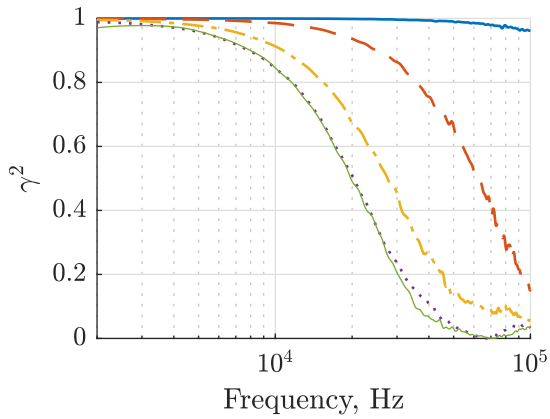

(e) Kevlar, −75° mic

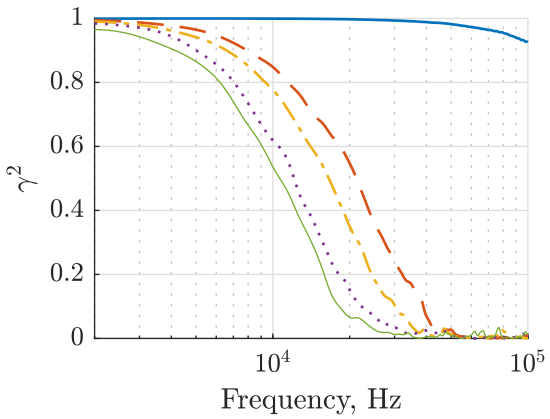

(f) Open-jet, −75° mic

Fig. 7 Comparison of γ^2 as a function of frequency between test section configurations for downstream angles. The reference microphone is at −90°.

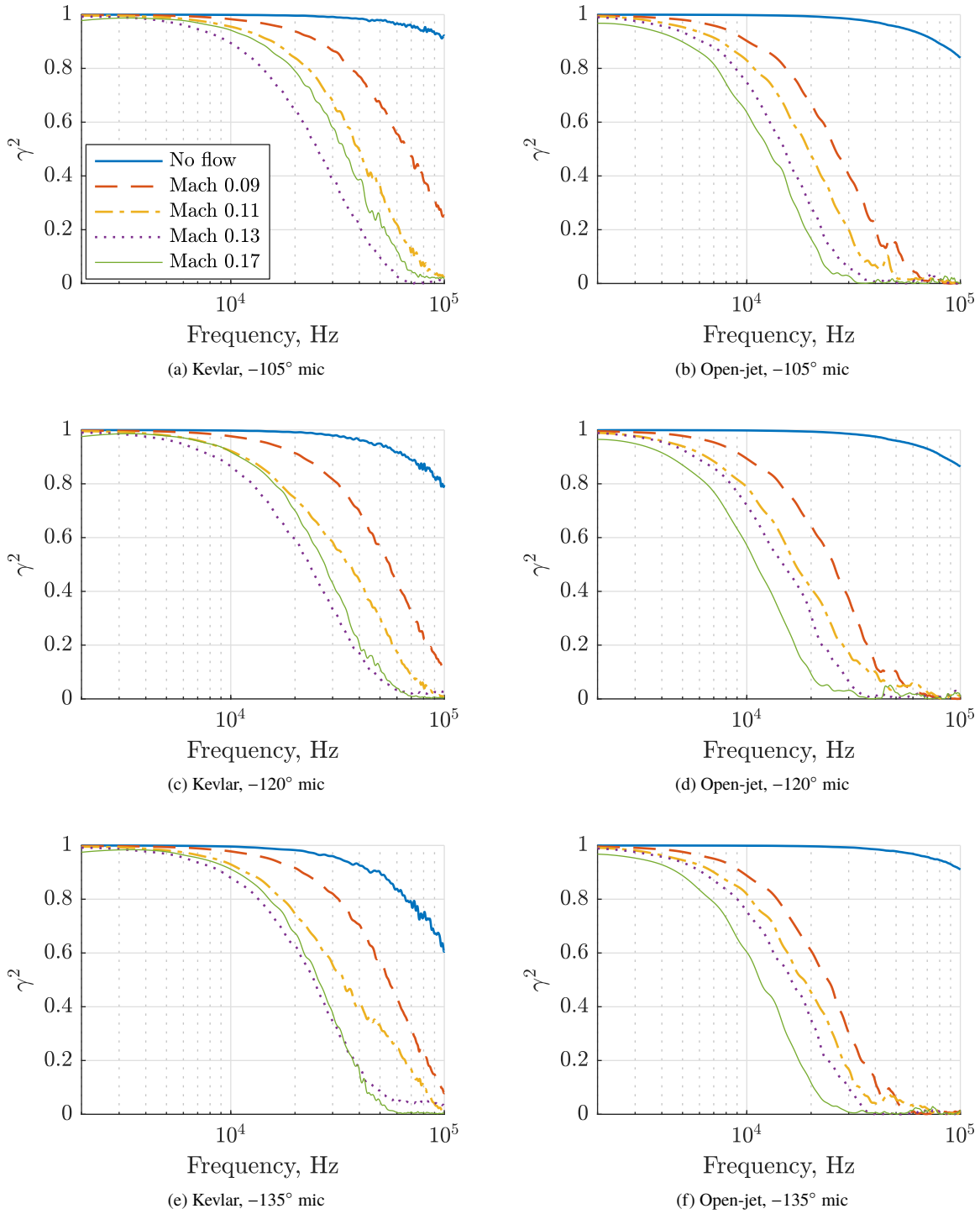

(a) Kevlar, −105° mic

(b) Open-jet, −105° mic

(c) Kevlar, −120° mic

(d) Open-jet, −120° mic

(e) Kevlar, −135° mic

(f) Open-jet, −135° mic

Fig. 8 Comparison of γ^2 as a function of frequency between test section configurations for upstream angles. The reference microphone is at −90°.

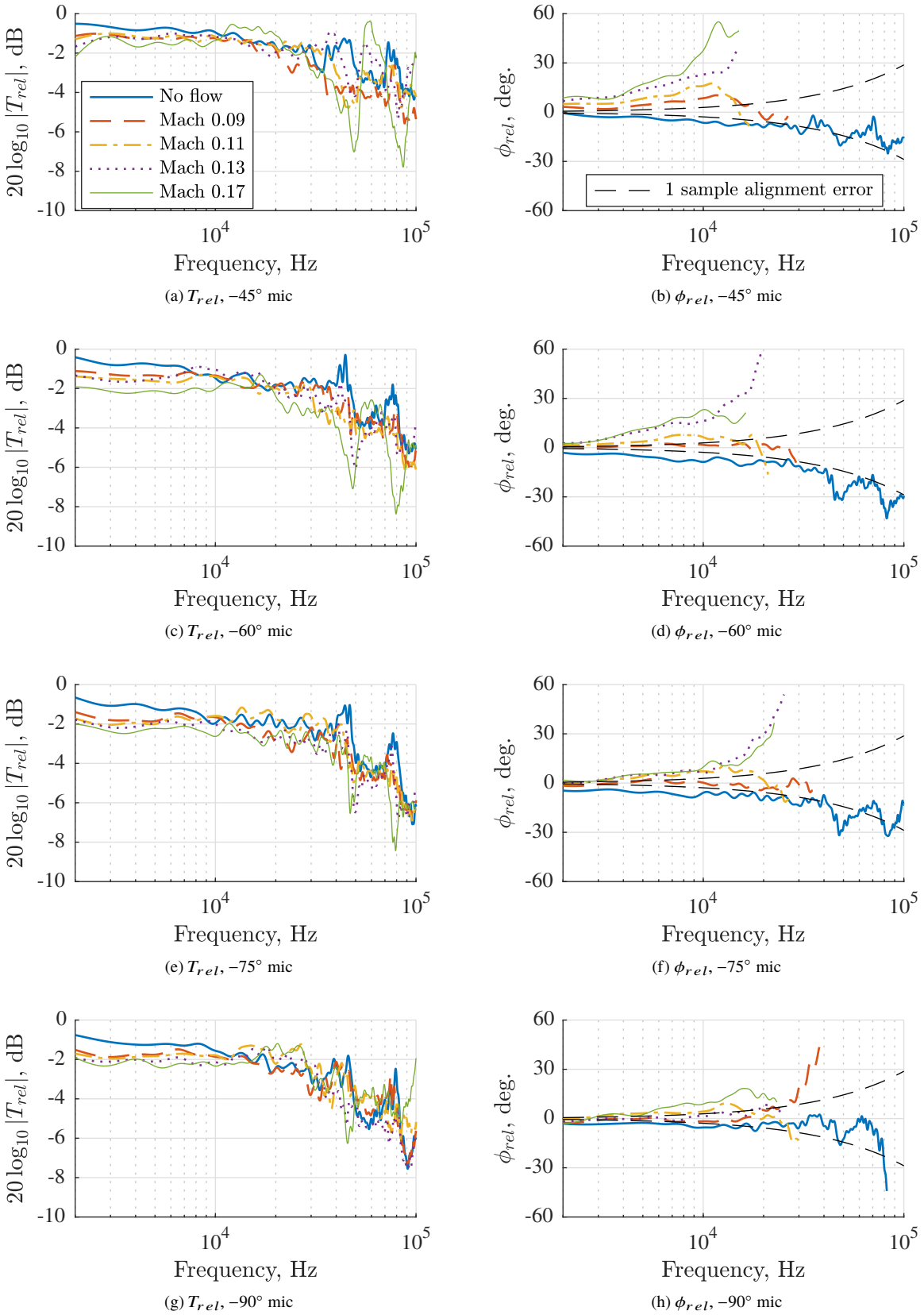

(a) T_{rel}, −45° mic

(b) ϕ_{rel}, −45° mic

(c) T_{rel}, −60° mic

(d) ϕ_{rel}, −60° mic

(e) T_{rel}, −75° mic

(f) ϕ_{rel}, −75° mic

(g) T_{rel}, −90° mic

(h) ϕ_{rel}, −90° mic

Fig. 9 Comparison of T_{rel} and ϕ_{rel} as a function of frequency and Mach number for downstream angles.

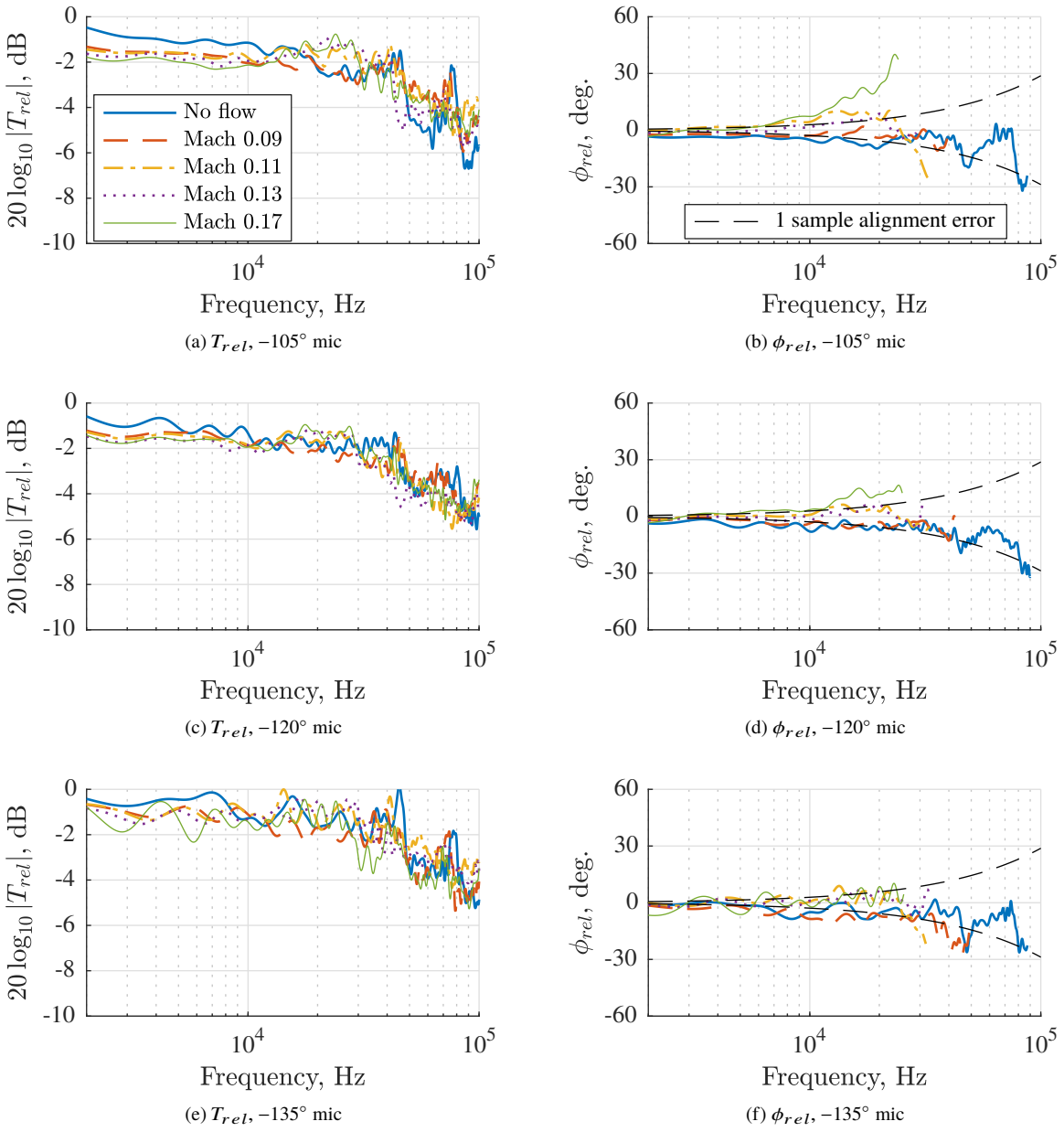

(a) T_{rel}, −105° mic

(b) ϕ_{rel}, −105° mic

(c) T_{rel}, −120° mic

(d) ϕ_{rel}, −120° mic

(e) T_{rel}, −135° mic

(f) ϕ_{rel}, −135° mic

Fig. 10 Comparison of T_{rel} and ϕ_{rel} as a function of frequency and Mach number for upstream angles.

Kevlar with respect to an open-jet configuration. Trends appear to be bounded within the 1-sample envelope, and for no flow actually appear to match the 1 sample delay bound. Downstream angles appear to experience a phase lead outside of this 1 sample envelope at higher Mach numbers. If real, this lead would suggest that the thicker open-jet shear layer is slowing down the signal as compared to the Kevlar. There are some significant phase excursions, but most of these appear where coherence is quite low and the uncertainty range is in the tens of degrees. One conclusion is that, once propagation delays have been accounted for, the Kevlar panel does not appear to induce any extreme phase shifts in acoustic transmission when compared to the open-jet configuration, in the average sense.

E. Autospectra and Background Noise

Autospectral densities of the signal are shown in Fig. 11 for a range of Mach numbers at an upstream, central, and downstream angle. For autospectral densities, the microphone directivity and actuator response do not cancel in calculations. Therefore these corrections [27] are applied to the data in addition to atmospheric attenuation. In general, the source appears to behave as a moving point source, matching the observations made in the companion shielding test [17]. There is a positive Doppler frequency shift in the downstream direction, the direction of source motion, and an increase in level with increasing Mach number. In the upstream direction there is a negative Doppler frequency shift and a reduction in level with increasing Mach number.

The spectra for the far downstream angle of -45° in the open-jet configuration appears to behave more erratically as compared to the Kevlar at the equivalent angle at Mach 0.17, when considering the frequency and magnitude of the dominant trough and secondary peak in the spectral shape. Similarly, this open-jet angle is more erratic than the other angles for both configurations. One possible cause of this, though unprovable with the current data, is that the turbulence in the free shear layer is sufficiently strong that the additional Doppler influence from eddy scattering is further spreading the spectrum [31]. This spreading affects the alignment of the spectra in the correction process from the previous section. When inspected visually, this misalignment of the secondary peak in the spectrum is found to drive the large peak and trough structures in the T_{rel} and ϕ_{rel} plots for downstream angles in Fig. 9. This Doppler misalignment does not appear in the upstream angle autospectra in Fig. 11 or corrections in Fig. 10.

Finally, (uncorrected) background noise autospectral densities for the two configurations are shown in Fig. 12. Only one angle is shown, as all angles show approximately the same behavior. These data were acquired by simply turning the laser system off for a given test condition with both configurations. Note that the measurement system noise floor is evident in almost all datasets at some frequencies, and completely dominates the no flow data. This is because the data acquisition system ranges and amplifier gains were set to acquire the laser pulse signal, not to measure an accurate facility acoustic noise floor. The gains could be increased by another 20 dB for a pure background noise measurement. Also, the noise floor levels shown in these plots are not representative of the noise floor in the laser pulse analyses. As mentioned in the discussion of the pulse spread, the gating process applied to the pulse data significantly reduces background noise power in computed spectra.

This comparison is the only one where the open-jet configuration shows a clear advantage when compared to the Kevlar panel when considering aeroacoustic measurement interests. At lower frequencies, noise levels from the Kevlar and open-jet configurations are similar, and both approximately the same at 3 kHz for Mach 0.17. However, at higher frequencies, the Kevlar panel data dramatically diverge from the open-jet data. At 10 kHz, the Kevlar data are approximately 5 dB above the open-jet data. The difference peaks at 40 kHz, with the background noise produced by the Kevlar configuration over 25 dB higher than that produced by the open-jet configuration. Depending on the nature of a given test, the Kevlar panel could prove problematic when attempting to measure a low level acoustic source.

V. Summary and Recommendations

A test comparing the unsteady propagation characteristics of an acoustic pulse in two different configurations of aeroacoustic wind tunnels is presented. The test compared the open-jet configuration with the Kevlar wall configuration, using a laser-generated acoustic point source. The pulsed source allows for the isolation of the direct propagation path through a gating process, and can be studied in terms of wander and spread. Metrics for these based on the current test are proposed, along with potential correction techniques.

By all proposed assessment metrics, the Kevlar panel configuration experiences far less unsteady influence on propagation from the source to the microphones. The spread of the pulses, or waveform distortion, is minimal with the Kevlar configuration, particularly when compared to the open-jet configuration. The wander, or variation in pulse arrival time, is also less with the Kevlar panel than with the open-jet configuration. These two characteristics drive the coherence behavior of the two configurations, where the Kevlar panel shows reduced decorrelation effects when

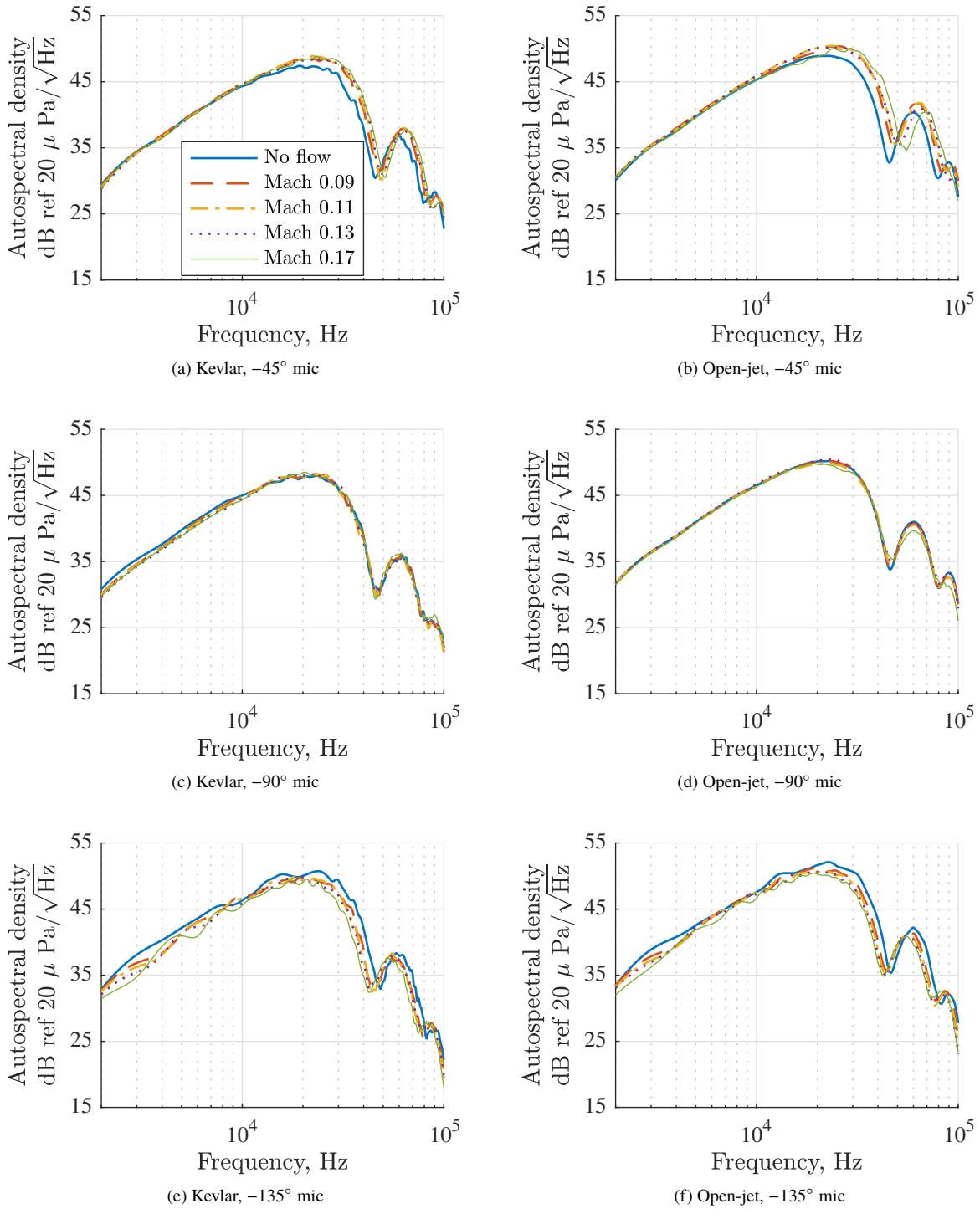

(a) Kevlar, −45° mic

(b) Open-jet, −45° mic

(c) Kevlar, −90° mic

(d) Open-jet, −90° mic

(e) Kevlar, −135° mic

(f) Open-jet, −135° mic

Fig. 11 Corrected autospectral densities of pulse waveforms for varying angle and Mach number.

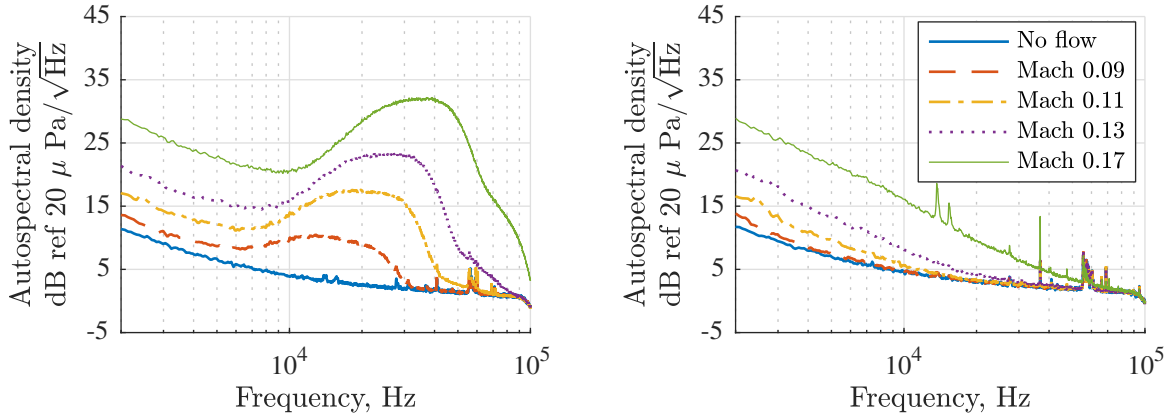

(a) Kevlar, −60° mic

(b) Open-jet, −60° mic

Fig. 12 Background autospectral densities of the two configurations as a function of Mach number.

compared to an open-jet configuration.

Relative corrections between the configurations are proposed and calculated. These corrections (as calculated in this test) are influenced by possible structural response of the Kevlar panel in combination with Doppler effects, making true quantitative analysis difficult. However, the data allow for qualitative discussion of the corrections. The overall magnitude correction trends with previous work, though the specific levels may be in disagreement. It shows little dependence on directivity and Mach number. This is likely because the magnitude correction is relative, so these directivity effects are common between the open-jet and Kevlar panel configurations. The phase angle correction suffers from coherence breakdown, but does show that phase angle corrections are low at low frequencies, and are, in many cases, bound by sampling time uncertainty at higher frequencies. Individual spectra confirm the Doppler behavior of the signal, and show that the Kevlar panel generates significantly more background noise than the open-jet at higher frequencies.

For a future test, the choice between Kevlar and open-jet configurations must be determined by the test requirements. Previous work has repeatedly shown that if a wind tunnel model will generate a significant amount of lift, Kevlar walls are far preferable to an open-jet. However, when high lift is not a concern, the source and measurement plan of interest should drive the decision process. For a measurement scheme where coherence is critical, Kevlar appears to be the superior choice. All of the unsteadiness metrics are far lower for the Kevlar panel than they are for the open-jet configuration. This would suggest that microphone phased arrays, for example, would benefit more from the Kevlar configuration than the open-jet configuration. Similarly, a test plan with distributed coherent sources should consider utilizing Kevlar walls. Conversely, if an aeroacoustic source of interest is particularly quiet, an open-jet configuration may be considered. The background noise production of the Kevlar is sufficiently high such that it could completely mask a 40 kHz source which is perfectly visible otherwise. The extent of spatial coherence for the source should still be considered here. A quiet source measurement which either has a large amount of source spatial coherence or is being acquired by a microphone phased array with large microphone spacings will prove challenging in either configuration.

Acknowledgments

The authors would like to acknowledge Dr. Russell Thomas of NASA Langley Research Center for leading the overall task and NASA contribution to the NATO effort, as well as funding by the NASA Advanced Air Transport Technology Project.

References

[1] Soderman, P. T., and Allen, C. S., "Microphone Measurements In and Out of Airstream," *Aeroacoustic Measurements*, edited by T. J. Mueller, Springer-Verlag, Berlin, Heidelberg, New York, 2002.

[2] Devenport, W. J., Burdisso, R. A., Borgoltz, A., Ravetta, P. A., Barone, M. F., Brown, K. A., and Morton, M. A., "The

Kevlar-walled anechoic wind tunnel," *Journal of Sound and Vibration*, Vol. 332, No. 17, 2013, pp. 3971–3991.

[3] Miles, J. W., "On the Reflection of Sound at an Interface of Relative Motion," *The Journal of the Acoustical Society of America*, Vol. 29, No. 2, 1957, pp. 226–228.

[4] Amiet, R. K., "Refraction of Sound by a Shear Layer," *Journal of Sound and Vibration*, Vol. 58, No. 4, 1978, pp. 467–482.

[5] Ostashev, V. E., and Wilson, D. K., *Acoustics in Moving Inhomogeneous Media*, CRC Press, Taylor & Francis Group, LLC, Boca Raton, Florida, 2016, Chap. 6: Random inhomogeneities in a moving medium and scattering of sound, pp. 187–222.

[6] Michel, U., "On the systematic error in measurements of jet noise flight effects using open jet wind tunnels," *21st AIAA/CEAS Aeroacoustics Conference*, AIAA 2015-2996, Dallas, Texas, 22–26 June 2015.

[7] Dougherty, R. P., "Turbulent Decorrelation of Aeroacoustic Phased Arrays: Lessons from Atmospheric Science and Astronomy," *9th AIAA/CEAS Aeroacoustics Conference*, AIAA 2003-3200, Hilton Head, South Carolina, 12–14 May 2003.

[8] Pires, L. S., Dougherty, R. P., Gerges, S. N. Y., and Catalano, F., "Predicting Turbulent Decorrelation in Acoustic Phased Array," *50th AIAA Aerospace Sciences Meeting*, AIAA 2012-0387, Nashville, Tennessee, 9–12 January 2012.

[9] Ernst, D., Spehr, C., and Berkefeld, T., "Decorrelation of Acoustic Wave Propagation through the Shear Layer in Open Jet Wind Tunnel," *21st AIAA/CEAS Aeroacoustics Conference*, AIAA 2015-2976, Dallas, Texas, 22–26 June 2015.

[10] Bahr, C. J., and Horne, W. C., "Subspace-based background subtraction applied to aeroacoustic wind tunnel testing," *International Journal of Aeroacoustics*, Vol. 16, No. 4–5, 2017, pp. 299–325.

[11] Hutcheson, F. V., Spalt, T. B., Brooks, T. F., and Plassman, G. E., "Airframe noise from a hybrid wing body aircraft configuration," *International Journal of Aeroacoustics*, Vol. 16, No. 7–8, 2017, pp. 540–562.

[12] Liu, C. H., and Yeh, K. C., "Pulse spreading and wandering in random media," *Radio Science*, Vol. 14, No. 5, 1979, pp. 925–931.

[13] Ostashev, V. E., Wilson, D. K., Collier, S. L., Cain, J. E., and Cheinet, S., "Cross-frequency coherence and pulse propagation in a turbulent atmosphere," *The Journal of the Acoustical Society of America*, Vol. 140, No. 1, 2016, pp. 678–691.

[14] Sijtsma, P., "Acoustic array corrections for coherence loss due to the wind tunnel shear layer," Tech. Rep. NLR-TP-2008-112, NLR, February 2008.

[15] Rossignol, K.-S., and Delfs, J., "Analysis of the Noise Shielding Characteristics of a NACA0012 2D Wing," *22nd AIAA/CEAS Aeroacoustics Conference*, AIAA 2016-2795, Lyon, France, 30 May – 1 June 2016.

[16] Rossignol, K.-S., Pott-Pollenske, M., Delfs, J., Silbermann, J., and Gomes, J., "Investigating Noise Shielding by Unconventional Aircraft Configurations," *23rd AIAA/CEAS Aeroacoustics Conference*, AIAA 2017-3195, Denver, Colorado, 5–9 June 2017.

[17] Hutcheson, F. V., Bahr, C. J., Thomas, R. H., and Stead, D. J., "Experimental Noise Shielding Study for a NACA 0012 Airfoil," *24th AIAA/CEAS Aeroacoustics Conference*, accepted for publication, Atlanta, Georgia, 25–29 June 2018.

[18] Qin, Q., and Attenborough, K., "Characteristics and application of laser-generated acoustic shock waves in air," *Applied Acoustics*, Vol. 65, No. 4, 2004, pp. 325–340.

[19] Bahr, C., Zawodny, N. S., Yardibi, T., Liu, F., Wetzel, D., Bertolucci, B., and Cattafesta, L., "Shear layer time-delay correction using a non-intrusive acoustic point source," *International Journal of Aeroacoustics*, Vol. 10, No. 5–6, 2011, pp. 497–530.

[20] Bahr, C. J., Zawodny, N. S., Bertolucci, B., Li, J., Sheplak, M., and Cattafesta, L. N., "A plasma-based non-intrusive point source for acoustic beamforming applications," *Journal of Sound and Vibration*, Vol. 344, 2015, pp. 59–80.

[21] Wright, W. M., "Propagation in air of *N* waves produced by sparks," *The Journal of the Acoustical Society of America*, Vol. 73, No. 6, 1983, pp. 1948–1955.

[22] Yuldashev, P., Ollivier, S., Averiyanov, M., Sapozhnikov, O., Khokhlova, V., and Blanc-Benon, P., "Nonlinear propagation of spark-generated *N*-waves in air: Modeling and measurements using acoustical and optical methods," *The Journal of the Acoustical Society of America*, Vol. 128, No. 6, 2010, pp. 3321–3333.

[23] Dougherty, R. P., "Advanced Time-domain Beamforming Techniques," *10th AIAA/CEAS Aeroacoustics Conference*, AIAA 2004-2955, Manchester, Great Britain, 10–12 May 2004.

[24] Lipkens, B., and Blackstock, D. T., "Model experiment to study sonic boom propagation through turbulence. Part I: General results," *The Journal of the Acoustical Society of America*, Vol. 103, No. 1, 1998, pp. 148–158.

[25] Averiyanov, M., Ollivier, S., Khokhlova, V., and Blanc-Benon, P., "Random focusing of nonlinear acoustic *N*-waves in fully developed turbulence: Laboratory scale experiment," *The Journal of the Acoustical Society of America*, Vol. 130, No. 6, 2011, pp. 3595–3607.

[26] Pascioni, K., Colangelo, A., and Cattafesta, L., "Acoustic Corrections for a Kevlar Wall Wind Tunnel Using a Pulsed-Laser Point Source," *24th International Congress on Sound and Vibration*, London, United Kingdom, 23–27 July 2017.

[27] *Condenser Microphones and Microphone Preamplifiers for acoustic measurements*, Brüel & Kjær, 1982.

[28] *Method for Calculation of the Absorption of Sound by the Atmosphere*, ANSI S1.26-1995 (ASA 113-1995), Acoustical Society of America, 1995.

[29] Koop, L., Ehrenfried, K., and Kröber, S., "Investigation of the systematic phase mismatch in microphone-array analysis," *11th AIAA/CEAS Aeroacoustics Conference*, AIAA 2005-2962, Monterey, California, 23–25 May 2005.

[30] Bendat, J. S., and Piersol, A. G., *Random Data Analysis and Measurement Procedures*, 3rd ed., John Wiley & Sons, Inc., New York, NY, 2000.

[31] Schlinker, R. H., and Amiet, R. K., "Refraction and Scattering of Sound by a Shear Layer," Tech. Rep. NASA-CR-3371, United Technologies Research Center, 1981.